

Fracture and deformation in brittle solids: A perspective on the issue of scale

Brian R. Lawn

Materials Science and Engineering Laboratory, National Institute of Standards and Technology, Gaithersburg, Maryland 20899-8500

(Received 12 June 2003; accepted 15 September 2003)

A perspective on the issue of scale in the fracture and deformation properties of ordinarily brittle covalent–ionic solids (ceramics) is presented. Characteristic scaling dimensions for nanomechanical properties of this class of solids are identified—specimen size or layer thickness, microstructural scale, and contact dimension. Transitions in mechanical damage processes occur as the characteristic dimensions diminish from the macroscale to the submicroscale. Such transitions generally preclude unconditional extrapolations of macroscopic-scale fracture and deformation laws into the nanomechanics region. Strength of brittle solids tends to increase while toughness tends to decrease as the scaling dimensions diminish. The nature of flaws that control strength in the submicroscale region also undergoes fundamental changes—even flaws without well-developed microcracks can be deleterious to strength.

I. INTRODUCTION

Materials technology is witnessing an ever-continuing miniaturization in microelectromechanical systems (MEMS) and nanoelectromechanical systems (NEMS), computer chips, sensors and actuators, microfluidics and bioengineering devices, and so on. Figure 1, a polysilicon MEMS device fabricated at the Sandia National Laboratories, is an illustrative example—characteristic dimensions of individual components, of component/component contacts, and of the underlying grain microstructures all lie in the submicrometer range. Questions inevitably arise as to how valid it is to extrapolate our knowledge base downward from the large scale as such characteristic dimensions diminish. We might expect to find fundamental differences between conventional responses at the macroscale (governed by continuum laws), microscale (governed by discrete defects—dislocations, microstructural interfaces, microcracks), and nanoscale (governed by interatomic force laws). Feynman, in his celebrated 1959 lecture “There Is Plenty of Room at the Bottom,” pointed out that properties will inevitably change on approaching the nanoscale, not just because of quantum effects but also from a shifting balance between competing classical forces as the surface/volume ratio increases. In this view, intrinsic size effects may be expected to constitute the rule rather than the exception in materials properties.

Size effects are no less true of mechanical properties. The mechanical properties of materials is a well-established field of study at the macroscale level. But

how valid are the conventional laws of fracture and deformation at the nanoscale—the realm of nanomechanics? How does diminishing separation between boundaries (external surfaces, internal grain or interlayer interfaces) increasingly constrain deformation and fracture processes? Are there fundamental transitions in underlying mechanisms en route between scaling limits? For instance, metals tend to become more brittle as grain or interlayer size diminishes.¹ This is attributable at least in part to an increasing hardness with diminishing grain size—Hall–Petch behavior²—as dislocation activity becomes progressively impeded at internal boundaries. There is also some suggestion of a reverse transition to softening at ultrasmall grain sizes, possibly associated with the proliferation of boundary-related slip sources. Fracture strength in ceramics shows an analogous increase with diminishing grain size.³ In this material class too there are some suggestions of strengthening processes at the nanoscale (e.g., in ceramic nanocomposites from intrinsic toughening mechanisms associated with nanoparticulates), augmented by internal residual stresses.⁴ In devices, especially systems with moving parts, material components are subject to small-scale contacts during fabrication, handling, or operation (e.g., Fig. 1). Even though the contact forces are typically small, they are highly concentrated, so attendant stresses may be sufficiently intense to introduce highly localized but deleterious damage that can cause premature failure.⁵ What is the nature of such damage as we enter the small-scale contact region, and how does it impact strength properties?

Thus, there are many questions that need to be addressed in the interest of ensuring reliability and performance of next-generation small-scale devices. In this paper we present a perspective on this topic, with a focus on mechanical properties of inherently brittle solids characterized by covalent/ionic bonding (i.e., ceramics and glasses). In such solids, the principal material property of interest in the nanoscale region is strength or some analogous critical fracture load. We will argue that these properties do indeed undergo fundamental transitions as scaling dimensions diminish, so that simple extrapolations into the nanoscale are not generally valid. Specific consideration will be given to three scaling variables: specimen size or layer thickness, microstructural scale, and contact dimension. Contact testing will be used as a simple test probe to quantify essential mechanical responses.

II. SPECIMEN SIZE

A. Monoliths—nature of flaws

As indicated above, materials components in devices are becoming ever smaller, with at least one dimension in the submicrometer region. These components are usually monocrystalline or fine-grain polycrystalline, sometimes glassy, with near-pristine surfaces. The first strength tests on brittle materials with such characteristics were made by Griffith in 1920 on freshly drawn glass fibers. Griffith's tests demonstrated that strengths well above 1 GPa, approaching the theoretical limit $E/10$ (E = Young's

modulus), were possible on pristine surfaces, but degraded steadily with aging and handling due to the incubation of submicroscopic flaws.⁶ The flaw size c_f relates to strength S according to the Griffith relation

$$S = T/\psi c_f^{1/2} \quad (1)$$

where T is toughness and ψ is a flaw geometry constant. Subsequent development of ultra-high-strength (>1 GPa) silica glass fibers with polymer coatings to prevent the inception of large flaws from the action of external agents has successfully been exploited by the optical fiber communications industry.

More recently, strength tests have been conducted on MEMS and semiconductor materials, principally polycrystalline or single-crystal silicon, fashioned in the form of rods, bars, or plates by photolithography or comparable fabrication technology.^{7,8} Such tests are simple in concept, although they can be experimentally demanding and costly. Generally, S increases into the GPa range as the limiting specimen dimensions diminish into the submicrometer region. An illustrative data set from some work by Namazu et al.⁷ on single-crystal silicon rods with diameters ranging from millimeters down to nanometers and loaded in flexure using an atomic force microscopy tip is shown in Fig. 2. Interestingly, not only does the mean strength increase in the nanoregion, but so does the Weibull modulus. The flaw size in the silicon can be calculated by inserting $T \sim 1 \text{ MPa}\cdot\text{m}^{1/2}$ and $\psi \sim 1$ into Eq. (1), yielding $c_f \sim 1 \text{ }\mu\text{m}$ at $S \sim 1 \text{ GPa}$.

The data trends in Fig. 2 are typical of specimen miniaturization and raise issues concerning flaw populations. Why are the flaws actually smaller in small-scale specimens? Is it just a matter of eliminating flaws in a large

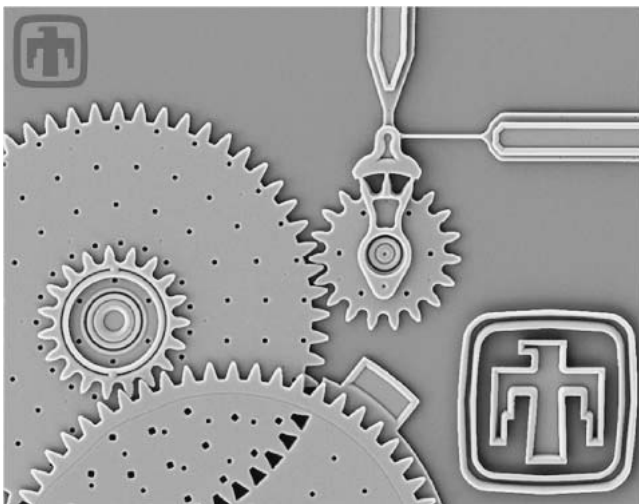


FIG. 1. Micrograph of MEMS device. Characteristic dimensions of component parts, internal grain structure, and intercomponent contact all lie in the submicrometer region. How well do conventional laws of mechanics apply at these and small dimensions? Width of field about 200 μm . Reproduced from the Sandia National Laboratories Web page.

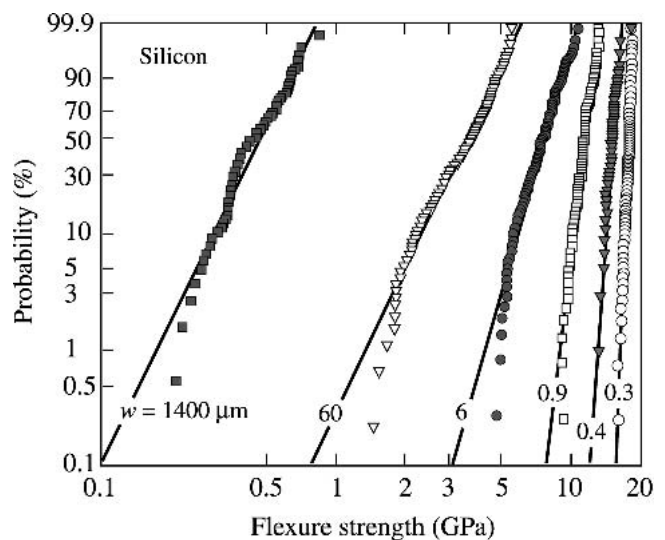


FIG. 2. Weibull strengths of silicon test specimens for bars of different characteristic mean cross-section widths w as indicated (μm). Mean strength and Weibull modulus increase with diminishing specimen size. Data reproduced from Ref. 7.

statistical distribution as the surface area diminishes? What is the fundamental nature of the flaws? How do they evolve, and are they truly crack-like as in large-scale specimens? There is a need to understand flaw mechanics more fully in the small-scale region.

We will return to the issue of the nature of small-scale flaws in Sec. IV.

B. Coatings and films—layer thickness

Analogous size effects are associated with diminishing layer thicknesses in coating and film structures. In metal coatings and multilayers, hardness increases with decreasing layer thickness as slip processes become more constrained.^{9–11} Here we focus on brittle layers on compliant (polymer) or soft (metal) substrates. Such systems are relevant to certain natural structures—shells, teeth, and bone—as well as to engineering structures—wear-resistant coatings, laminated windows, and eyeglasses.^{12–14} Whereas considerable effort is now being directed by the nanotechnology community toward the failure of ultrathin brittle films, links between mechanics and mechanisms at the macroscale and nanoscale remain obscure.

Consider the axisymmetric bilayer system in Fig. 3, consisting of a brittle layer of thickness d on a thick compliant substrate, with a contact force P acting over a radius a at the top surface. The assumption of a fixed (nonzero) contact area ensures elastic deformation up to a critical load for fracture (“blunt” contact¹⁵), thereby simplifying the analysis. Three regions of relative thickness d/a are identified in Fig. 3.

(I) *Thick coatings*. The system behaves as a brittle monolith, with the stresses concentrated at the top surface. Fracture occurs as a near-axisymmetric cone crack close to the contact circle, where the tensile stresses are a maximum.¹⁴

(II) *Thin coatings*. The coating begins to flex, and the primary maximum in tensile stress shifts to the coating lower surface.¹⁶ Radial cracks initiate in the center region and propagate on median planes through the contact

axis. At the top surface, the peak tensile stress moves outward from the contact circle onto the shoulders, forming relatively shallow, secondary ring cracks.

(III) *Thin films*. Cracking becomes suppressed within the compression zone beneath the Hertzian contact, and the maximum tensile stresses shift back to the top surface close to the contact circle.^{16–18} Membrane stresses come increasingly into play. Overloading in any of these regions produces multiple cracking, including punch-in shear failures and delamination, especially when plasticity is induced in either the substrate or coating.^{16,17,19,20}

Fracture mechanics descriptions of each of these modes can be complex.¹⁴ However, conservative relations can be obtained by considering fracture to occur when the maximum tensile Hertzian stresses (region I), flexural stresses (region II) or thin film stresses (region III) equal the bulk strength S . This yields critical loads for surface cone cracks and subsurface radial cracks

$$P_C = ASa^2, \quad (\text{region I}) \quad (2a)$$

$$P_R = BSd^2/\log(CE/E_s), \quad (\text{region II}) \quad (2b)$$

$$P_C = ASa^2E_s/E, \quad (\text{region III}) \quad (2c)$$

where E and E_s are Young’s modulus of brittle layer and substrate and A , B , and C are dimensionless coefficients.²¹ Equations (2a) and (2c) are obtained from the relation for the maximum tensile stress at the contact circle (the latter with due allowance for an infinitesimally thin layer on a semi-infinite substrate), and Eq. (2b) from the theory for elastic plates on a compliant substrate.¹⁴ A plot of P_R/ASa^2 versus d/a calculated from Eq. (2) is shown as the solid lines in Fig. 4 for $E/E_s = 30$ (glass/polycarbonate). Points are corresponding data from finite element analysis (FEA) calculations for surface cone or ring cracking and radial cracking. The lower of these two data sets represents first cracking conditions, with the crossover points delineating regions I, II, and III in Fig. 3. In general, the FEA data lie somewhat above the simplistic predictions from Eq. (2), owing to the assumption of pure Hertzian contact in Eqs. (2a) and (2c)

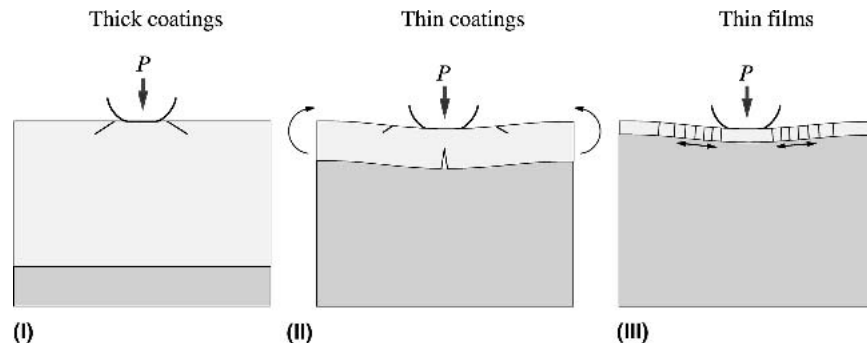


FIG. 3. Schematic of bilayer structure consisting of outer brittle layer of thickness d on thick compliant substrate, in axisymmetric contact on top surface at load P over a circular area of radius a (not shown). Showing fracture mode transitions in brittle layer: (I) cone crack at top surface (thick coatings), (II) ring crack at top surface and radial crack at bottom surface (thin coatings), and (III) concentric through-thickness ring cracks (thin films).

(neglecting flexure contributions) and the assumption of a nonzero contact area in Eq. (2b) (C dependent on d/a).²² Actual experimental data may lie even higher on such plots, from additional constraining effects of stress gradients^{23,24} and flaw statistics.²⁵ Notwithstanding such deviations, Eq. (2) remains a useful lower bound to actual behavior of brittle layer systems in concentrated loading.

These results demonstrate that size effects may be rendered as transitions in fracture mechanisms with diminishing relative coating thickness d/a . We have illustrated with just one loading system, but such transitions may be expected to be the rule rather than the exception. Downward extrapolations are therefore not generally viable. Again, the need to focus more on the region of ultrathin

films, where yet more mechanisms may kick in, is manifest.

III. MICROSTRUCTURAL SCALE

Another scale that has a profound effect on strength properties is grain size (or other characteristic microstructural dimension). Generally, the stresses needed to induce fracture (or yield) increase with an approximate (grain size)^{-1/2} dependence (Hall–Petch). The refinement of polycrystalline ceramic (and metal) structures into the nanoregion has been a strong driving force in the quest for ultra-high-strength materials.⁴ The simplistic picture is one of reducing the scale of the grain-localized flaws inherently associated with weak interfaces (grain boundaries, twins, and so forth) in the microstructure.⁵ However, not all properties may benefit from microstructural refinement, so due caution needs to be exercised in materials design.

This last point can be demonstrated by examining the indentation response of polycrystalline ceramics as a function of microstructural scale. The example in Fig. 5 is for sphere indentations on the surfaces of a micaceous glass-ceramic (MGC) at two microstructural scales:^{26–28} (a) fine microstructure (grain size $l \approx 1 \mu\text{m}$), showing a tensile cone crack (“brittle” response); and (b) coarse microstructure ($l \approx 10 \mu\text{m}$), showing a diffuse zone of closed shear microcracks (“quasiplastic” response). Increasing grain size introduces larger microcrack flaws by promoting frictional sliding at the weak mica/glass-matrix interfaces.^{29,30} It also toughens the material by inhibiting the growth of well-defined single cracks.²⁶ Such microstructure-controlled brittle–plastic transitions are observed to a greater or lesser degree in all polycrystalline ceramics.³¹

Thus, for any given ceramic, strength and toughness tend to have an inverse relationship.^{5,31} Considering

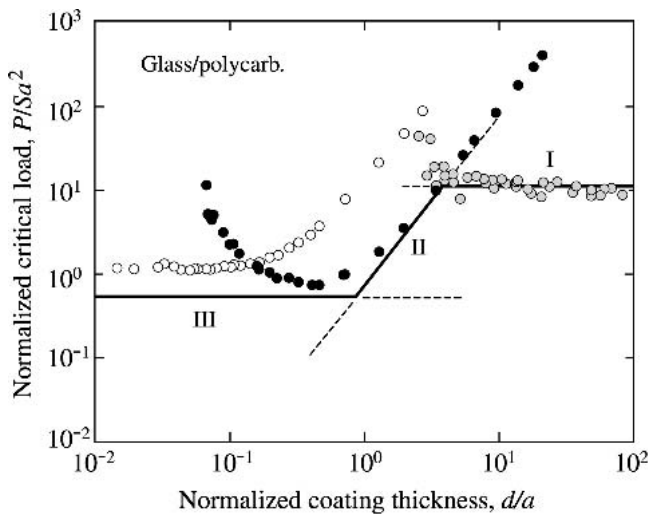


FIG. 4. Plot of normalized critical load P/Sa^2 versus d/a for coating/substrate modulus $E/E_s = 30$ (glass/polycarbonate). Solid lines are calculated from Eq. (2). Data points are FEA computations: surface ring cracks (unfilled symbols), cone cracks (partially filled symbols), and subsurface radial cracks (filled symbols). Regions I–III as indicated in Fig. 3. Data courtesy H. Chai.

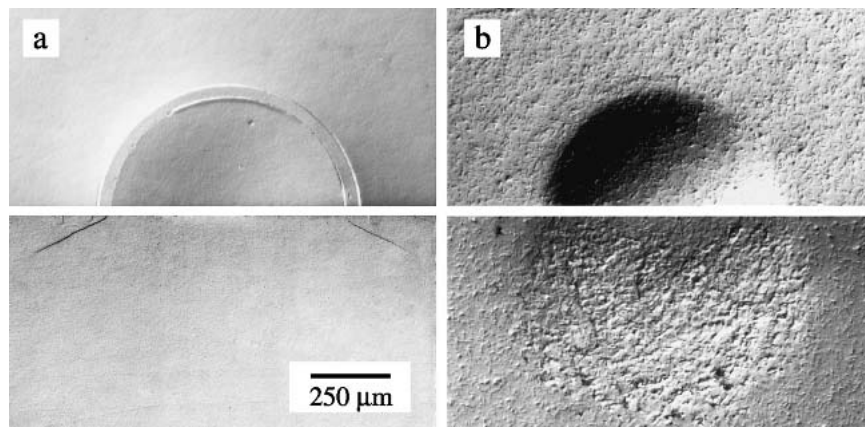


FIG. 5. Hertzian indentation damage in (a) fine-grain and (b) coarse-grain micaceous glass-ceramic, from WC sphere ($r = 1.98 \text{ mm}$, $P = 1000 \text{ N}$). Half-surface and side view of bonded-interface specimen, surfaces gold-coated after indentation, optical micrographs (Nomarski illumination). Reproduced from Ref. 26.

toughness first, ceramics generally exhibit R-curve behavior with enhancement of long-crack toughness T_∞ relative to short-crack toughness T_0 at larger grain sizes.³¹ Whereas T_0 is governed by intrinsic grain boundary or interface energies, T_∞ is augmented by dissipative crack-tip shielding processes, such as bridging by frictional grain pullout.³² It is usually T_∞ that is measured (as K_{IC}) in conventional fracture specimens. Data for T_∞ as a function of grain size l are shown in Fig. 6 for the MGC ceramic in Fig. 5, obtained using a single-edge-precracked-beam technique.³³ These data may be represented by $T_\infty(l) = T_0[1 + (l/L)^{1/2}]$, with L a characteristic grain-bridging dimension inversely dependent on Young's modulus and grain-sliding friction coefficient. A general conclusion that may be drawn from such data is that microstructural refinement will tend to diminish any toughening process.

Consider now the strength properties of the same glass-ceramic material. Data for surfaces in their as-polished state (filled symbols) and after predamage from spherical indenters at a prescribed load $P = 700$ N (unfilled symbols) are plotted in Fig. 7. These data were measured on bars in four-point bending, with the indentation sites in the predamaged specimens on the tensile side.²⁸ Taking the as-polished specimens first, S increases monotonically with decreasing l as expected. For this case, it can be supposed that the scale of the critical closed microcrack flaws is determined by the intrinsic grain size in the short-crack region; so that, inserting $T = T_0$ and $c = l$ into Eq. (1), we have

$$S = \psi T_0 / l^{1/2}, \quad (\text{as-polished}) \quad (3a)$$

Equation (3a) is plotted as the monotonically decreasing curve. Hall-Petch is obeyed, within the data scatter,

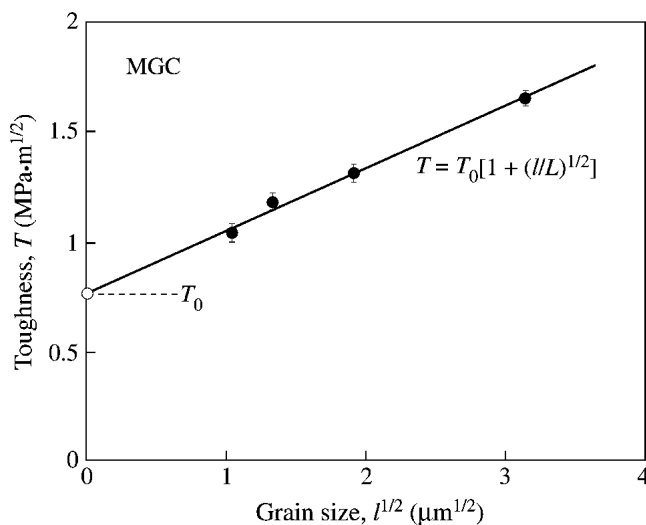


FIG. 6. Toughness as a function of square-root grain size for a micaceous glass-ceramic. Point on left axis represents base glass from which the glass-ceramic is processed. Data reproduced from Ref. 33.

over the grain size range covered. In the case of preindented surfaces, on the other hand, the strength data show a maximum at some intermediate grain size l^* . At $l > l^*$, the quasiplasticity mode prevails [Fig. 5(b)]—the closed microcracks extend incrementally at their ends as “wing cracks,”^{34,35} and S is only slightly diminished. Thus, Eq. (3a) remains an approximate upper bound. At $l < l^*$, the brittle mode prevails [Fig. 5(a)]—inserting $T = T_\infty(l)$ from above and $c = (\chi P/T_\infty)^{2/3}$ for cone cracks (χ another crack-geometry coefficient)^{31,36} into Eq. (1), we obtain

$$S = S_0[1 + (l/L)^{1/2}]^{4/3}, \quad (\text{as-indented}) \quad (3b)$$

where $S_0 \sim T_0^{4/3}/P^{1/3}$ is a lower strength limit at $l = 0$ (in this case for the base glass used to form the glass-ceramic). This equation is represented as the monotonically increasing curve in the figure. Thus again, a size-dependent brittle-plastic transition is evident.

Some general conclusions for polycrystalline ceramics may be drawn from the results in Fig. 7. Increasing the indentation preload P will lower both $S(l)$ curves in Eq. (3), but especially that in the brittle region of Eq. (3b), and thereby move the crossover point l^* to larger grain sizes. Such trends will be exacerbated by the use of sharper (e.g., Vickers) indenters. The region $l > l^*$ is the damage-tolerant domain of structural ceramics,³⁷ where dissipative processes operate and the main design requirement is the attainment of high toughness to contain long cracks. In this domain, ceramics are susceptible to gross wear from microcrack coalescence³⁸ and cyclic fatigue from loss of crack-tip shielding.^{39,40} The region $l < l^*$ is the more pertinent domain of advanced ceramics,

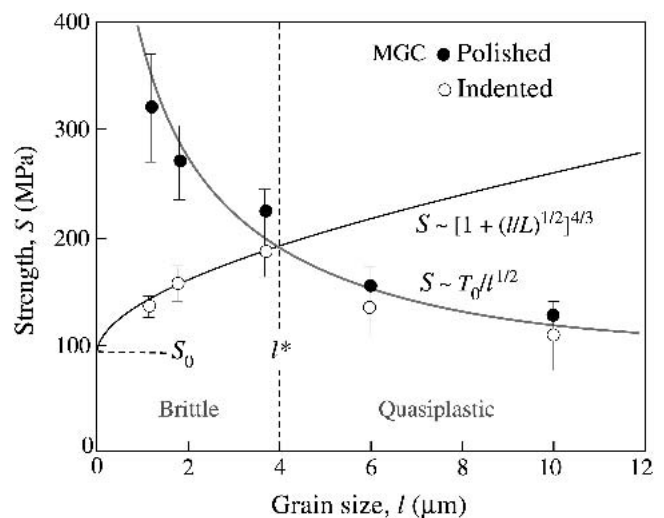


FIG. 7. Strength as a function of grain size for MGC materials. Filled symbols are breaks for specimens with polished surfaces; unfilled symbols from preindented surfaces (WC indenter, $r = 3.18$ mm and $P = 750$ N). Solid lines are asymptotic limits from Eq. (3). Grain size l^* delineates plastic-brittle response regions. Reproduced from Ref. 28.

where high strengths are attainable but damage tolerance is low. This is the domain of brittle fine-grain polycrystals and nanocomposites, where the principal goal is to avoid the incidence of any large flaws to maintain high strength levels (crack prevention). Some proponents of ceramic nanocomposites⁴ argue that it should be possible to increase strength and toughness simultaneously by designing structures with rapidly rising R-curves over very small crack extensions, effectively diminishing l^* into the submicrometer region. Others⁴¹ have argued that any such toughening is likely to be inconsequential, over and above the rule of mixtures; so that the main role of fine particulate additives in nanocomposites is to produce fine microstructures by inhibiting grain growth, thereby enhancing strength at the expense of toughness.

IV. CONTACT DIMENSION

Moving parts in devices are susceptible to damage from contacts, compromising performance and lifetime. Miniaturization of the devices commensurately reduces the size of such contacts (e.g., Fig. 1), concentrating the stresses and thereby increasing the potential for irreversible damage at ever-lower critical loads. For blunt (Hertzian) indentations, there exists a well-documented threshold sphere radius below which cracking is suppressed:^{23,42} above the threshold, cone cracks dominate; below the threshold, plasticity dominates. An analogous cracking threshold is observed for sharp (Vickers) indentations, in this case below a critical contact or penetration dimension.⁴³ Such thresholds are attributable to increasingly severe stress gradients within the ever-confining contact fields, most markedly in the tensile stresses, making it relatively difficult to initiate cracks.⁴⁴ Once more, a size-dependent brittle–plastic transition is manifest, this time as an indentation scaling effect.

In this section, we consider a worst-case situation, that of contacts from sharp (Vickers/Berkovich) indenters on ordinarily brittle materials with single-valued toughness

T_0 —monolithic glasses, single-crystal ceramics, and nanoscale polycrystalline ceramics. Sharp contacts can introduce damage in otherwise pristine surfaces at very low (\sim mN) loads. In pristine glass fibers, for instance, a single contact from a micrometer-scale dust particle can degrade strength by over an order of magnitude. At sharp contacts, cracking is invariably preceded by local “plasticity” within the hardness zone. The plasticity takes the form of punched-in discrete slip events, so-called shear faults,⁴⁵ at relatively high stress levels ($H/E > 0.1$).⁴⁶ These faults provide the embryonic flaws for initiation of corner radial cracks. An example of hardness-zone shear faults and ensuing radial cracks is shown in Fig. 8 for soda-lime glass.^{47,48} A characteristic of sharp contacts is that they generate their own flaws, even in initially defect-free materials (e.g., dislocation-free silicon), so that contact history totally controls the strength properties.

The threshold condition for sharp indenters can be determined from basic relations for the deformation and fracture dimensions:⁴⁴ for deformation, impression diagonal $a = (P/2H)^{1/2}$, where H is indentation hardness; for fracture, radial crack length $c = (\chi P/T_0)^{2/3}$, where $\chi = \xi(E/H)^{1/2}(\cot \varphi)^{2/3}$ is an elastic–plastic geometry coefficient³⁶ (φ = indenter half-angle). Because c varies more strongly than does a with load P , there is a critical dimension $a_* = c_*$ below which the radial crack is subsumed within the hardness zone:

$$a_* = (T_0/2\chi H)^2 \quad . \quad (4)$$

Above a_* fracture dominates, and below a_* plasticity dominates. Estimates of a_* range between 0.1 and 10 μm for typical brittle solids and Vickers indentations.⁵

Now consider the strength of initially pristine materials with surfaces containing sharp indentations. In the post-threshold cracking region, strength S in Eq. (1) is governed by radial crack size $c \sim (P/T_0)^{2/3} \sim (Ha^2/T_0)^{2/3}$,

$$S \sim T_0^{4/3}/H^{1/3}a^{2/3}, \quad (a > a_*) \quad . \quad (5a)$$

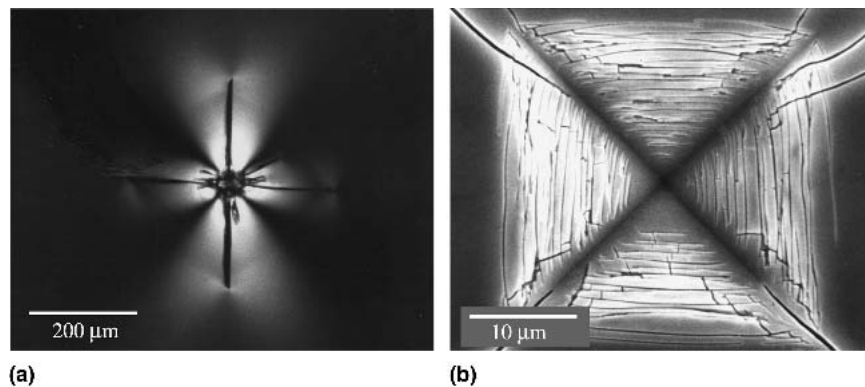


FIG. 8. Micrographs of Vickers indentations in soda-lime glass. (a) As-Indented surface, viewed in transmitted polarized light in crossed polars. Radial cracks emanate from impression corners, driven by residual stresses associated with plastic zone. (b) Indented surface after etching—discrete shear faults within hardness impression act as sources for the radial cracks. Below threshold impression size, radial cracks are suppressed. Reproduced from Refs. 47 and 48.

In the subthreshold plasticity region, strength is governed by the impression (shear fault) size a ,

$$S \sim T_0/a^{1/2}, \quad (a < a^*) \quad (5b)$$

Data for strength S for optical glass fibers containing Vickers flaws are plotted as a function of impression size a in Fig. 9.⁴⁹ The values of S either side of the threshold differ not only in magnitude, but also in the S - a exponent. Particularly noteworthy is the continual increase in S with diminishing a in the subthreshold region, attesting to the capacity of even submicroscopic flaws to degrade strength. Clearly, simple extrapolation of the conventional fracture mechanics into the submicrometer region is invalid.

Controlled indentation experiments of the kind described here provide some insights into the nature of contact-induced damage that may be incurred by device components in service. A schematic representation of a model derived from several studies of indentation damage in brittle solids is shown in Fig. 10.^{45,50-52} In hard ceramics, dislocation motion is inhibited by very high

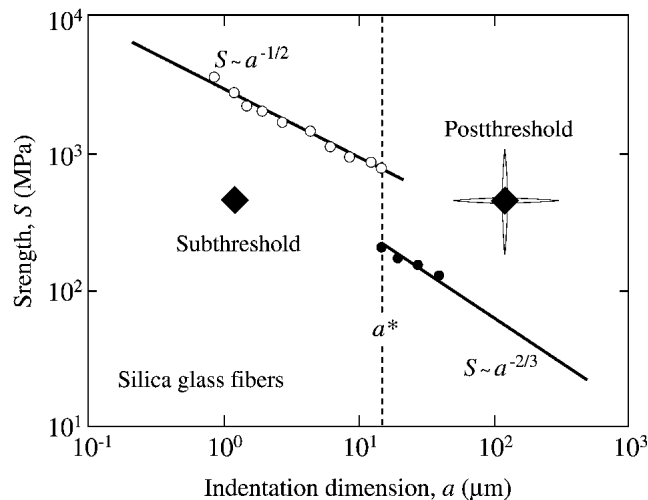


FIG. 9. Strength of silica fiber as function of Vickers indentation dimension. Tests conducted in liquid nitrogen. Data reproduced from Ref. 49.

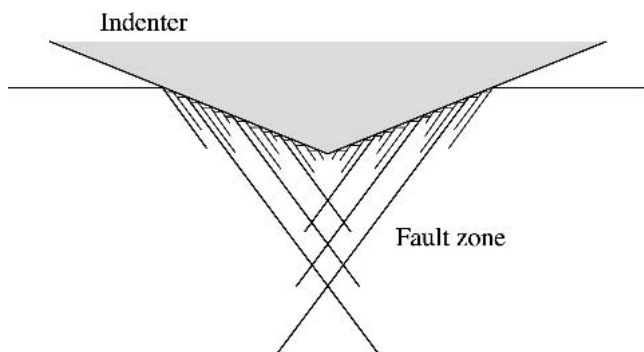


FIG. 10. Schematic of shear fault formation to accommodate penetration under Vickers indenter. Stress concentrations at intersections between fault surfaces can initiate radial cracks above threshold loads.

Peirels stresses, approaching the intrinsic cohesive strength of the structure ($\sim G/S$; G = shear modulus).⁵³ As the indenter begins to contact a specimen surface, the elastic stresses build up rapidly until the cohesive strength of the solid is exceeded. At that point a shear fault, akin to a shear crack with friction at the sliding interface, abruptly propagates into the subsurface, somewhat relaxing the contact pressure as it does so. As the indenter continues to penetrate, the stresses build up again, and the process repeats itself. Hence, the inherent discreteness in the fault patterns noted in Fig. 8(b). In isotropic materials such as glasses or fine-grain polycrystals, the fault surfaces follow curved shear stress trajectories; in single crystals, the faults follow more along weak crystallographic planes. A distinguishing feature of the fault patterns in ceramics (in contrast to metals) is their strong localization around the indentation site. Intersection lines between fault surfaces provide high stress concentration sites for initiation of ensuing radial cracks. Processes of this kind have recently been dramatically revealed beneath nanoindentations in semiconductor crystals using the transmission electron microscope.^{54,55}

More detailed experiments using the latest generation of high-resolution microscope facilities to examine contact processes, particularly using in situ testing stages,⁵⁶ should provide further insight into flaw generation processes. Other deleterious processes such as adhesion, friction (stiction), wear, and fatigue at the contact interface are likely to show analogous transitional behavior on entering the nanoscale.

V. CONCLUSIONS

(1) Characteristic scaling dimensions for nanomechanical properties of covalent-ionic solids (ceramics) have been identified. These include specimen size or layer thickness, microstructural scale, and contact dimension.

(2) Transitions in mechanical damage processes as characteristic dimensions diminish have been described. These include brittle-plastic transitions. Such transitions preclude unconditional extrapolation from macroscale properties into the nanoscale.

(3) Generally, strength increases and toughness decreases as the characteristic scaling dimensions in (1) diminish.

(4) The nature of flaws that control strength properties of brittle solids changes in the nanoscale region. Even flaws without well-developed cracks can be deleterious to strength.

ACKNOWLEDGMENTS

Useful discussions with Antonia Pajares and Herzl Chai are gratefully acknowledged. Information on product

names and suppliers in this paper is not to imply endorsement by NIST.

REFERENCES

1. E. Arzt, *Acta Mater.* **16**, 5611 (1998).
2. N.J. Petch, in *Fracture*, edited by H. Liebowitz (Academic Press, New York, 1968), Vol. 1, Chapter 5. p. 351.
3. R.W. Rice, *Proc. Br. Ceram. Soc.* **20**, 205 (1972).
4. T. Ohji, T. Jeong, Y.K. Choa, and K. Niihara, *J. Am. Ceram. Soc.* **81**, 1453 (1998).
5. B.R. Lawn, *Fracture of Brittle Solids* (Cambridge University Press, Cambridge, 1993).
6. A.A. Griffith, *Phil. Trans. Roy. Soc. Lond. A* **221**, 163 (1920).
7. T. Namazu, Y. Isono, and T. Tanaka, *Journal of Microelectromechanical Systems* **9**, 450 (2000).
8. J.N. Ding, Y.G. Meng, and S.Z. Wen, *J. Mater. Res.* **16**, 2223 (2001).
9. S.L. Lehoczky, *J. Appl. Phys.* **49**, 5479 (1978).
10. G.S. Was and T. Foecke, *Thin Solid Films* **286**, 1 (1996).
11. D. Josell, D.v. Heerden, D. Read, J. Bonevich, and D. Schechtman, *J. Mater. Res.* **13**, 2902 (1998).
12. W.W. Gerberich, A. Strojny, K. Yoder, and L-S. Cheng, *J. Mater. Res.* **14**, 2210 (1999).
13. B.R. Lawn, *Curr. Opin. Solid State Mater. Sci.* **6**, 229 (2002).
14. B.R. Lawn, Y. Deng, P. Miranda, A. Pajares, H. Chai, and D.K. Kim, *J. Mater. Res.* **17**, 3019 (2002).
15. B.R. Lawn and T.R. Wilshaw, *J. Mater. Sci.* **10**, 1049 (1975).
16. H. Chai, B.R. Lawn, and S. Wuttiphan, *J. Mater. Res.* **14**, 3805 (1999).
17. E. Weppelmann and M.V. Swain, *Thin Solid Films* **286**, 111 (1996).
18. R. Anderson, G. Toth, L. Gan, and M.V. Swain, *Eng. Fract. Mech.* **61**, 93 (1998).
19. N.B. Thomsen, A.C. Fischer-Cripps, and M.V. Swain, *Thin Solid Films* **332**, 180 (1998).
20. M.R. Begley, A.G. Evans, and J.W. Hutchinson, *Int. J. Solids Struct.* **36**, 2773 (1999).
21. H. Chai and B.R. Lawn, *J. Mater. Res.* (submitted).
22. S. Timoshenko and S. Woinowsky-Krieger, *Theory of Plates and Shells* (McGraw-Hill, New York, 1959).
23. F.C. Frank and B.R. Lawn, *Proc. Roy. Soc. Lond. A* **299**, 291 (1967).
24. H. Chai, *Int. J. Solids Struct.* **40**, 591 (2003).
25. P. Miranda, A. Pajares, F. Guiberteau, F.L. Cumbreira, and B.R. Lawn, *Acta Mater.* **49**, 3719 (2001).
26. H. Cai, M.A. Stevens-Kalceff, and B.R. Lawn, *J. Mater. Res.* **9**, 762 (1994).
27. A.C. Fischer-Cripps and B.R. Lawn, *J. Am. Ceram. Soc.* **79**, 2609 (1996).
28. I.M. Peterson, S. Wuttiphan, B.R. Lawn, and K. Chyung, *Dent. Mater.* **14**, 80 (1998).
29. A.C. Fischer-Cripps and B.R. Lawn, *Acta Mater.* **44**, 519 (1996).
30. A.C. Fischer-Cripps, *J. Am. Ceram. Soc.* **84**, 2603 (2001).
31. B.R. Lawn, *J. Am. Ceram. Soc.* **81**, 1977 (1998).
32. P.L. Swanson, C.J. Fairbanks, B.R. Lawn, Y-W. Mai, and B.J. Hockey, *J. Am. Ceram. Soc.* **70**, 279 (1987).
33. J.B. Quinn, V. Sundar, and I.K. Lloyd, *Dent. Mater.* (2003).
34. H. Horii and S. Nemat-Nasser, *Phil. Trans. Roy. Soc. Lond.* **19**, 603 (1986).
35. B.R. Lawn, S.K. Lee, I.M. Peterson, and S. Wuttiphan, *J. Am. Ceram. Soc.* **81**, 1509 (1998).
36. B.R. Lawn, A.G. Evans, and D.B. Marshall, *J. Am. Ceram. Soc.* **63**, 574 (1980).
37. A.G. Evans, *J. Am. Ceram. Soc.* **73**, 187 (1990).
38. S-J. Cho, B.J. Hockey, B.R. Lawn, and S.J. Bennison, *J. Am. Ceram. Soc.* **72**, 1249 (1989).
39. S. Lathabai, J. Rödel, and B.R. Lawn, *J. Am. Ceram. Soc.* **74**, 1340 (1991).
40. R.O. Ritchie, *Int. J. Fract.* **100**, 55 (1998).
41. J.H. Zhao, L.C. Stearns, M.P. Harmer, H.M. Chan, G.A. Miller, and R.F. Cook, *J. Am. Ceram. Soc.* **76**, 503 (1993).
42. Y-W. Rhee, H-W. Kim, Y. Deng, and B.R. Lawn, *J. Am. Ceram. Soc.* **84**, 561 (2001).
43. B.R. Lawn and A.G. Evans, *J. Mater. Sci.* **12**, 2195 (1977).
44. B.R. Lawn and D.B. Marshall, *J. Am. Ceram. Soc.* **62**, 347 (1979).
45. B.R. Lawn, T.P. Dabbs, and C.J. Fairbanks, *J. Mater. Sci.* **18**, 2785 (1983).
46. B.R. Lawn and V.R. Howes, *J. Mater. Sci.* **16**, 2745 (1981).
47. T.P. Dabbs, C.J. Fairbanks, and B.R. Lawn, in *Methods for Assessing the Structural Reliability of Brittle Materials*, edited by S.W. Freiman and C.M. Hudson (ASTM Special Technical Publication 844, Philadelphia, 1984), pp. 142–53.
48. D.H. Roach, S. Lathabai, and B.R. Lawn, *J. Am. Ceram. Soc.* **71**, 97 (1988).
49. B. Lin and M.J. Matthewson, *Philos. Mag. A* **74**, 1235 (1996).
50. M.J. Hill and D.J. Rowcliffe, *J. Mater. Sci.* **9**, 1569 (1974).
51. J.T. Hagan, *J. Mater. Sci.* **14**, 2975 (1979).
52. J.T. Hagan, *J. Mater. Sci.* **15**, 1417 (1980).
53. A. Kelly, *Strong Solids* (Clarendon Press, Oxford, 1966).
54. J.G. Bradby, J.S. Williams, J. Wong-Leung, M.V. Swain, and P. Munroe, *J. Mater. Res.* **16**, 1500 (2001).
55. J.G. Bradby, J.S. Williams, J. Wong-Leung, S.O. Kucheyev, M.V. Swain, and P. Munroe, *Philos. Mag. A* **82**, 1931 (2002).
56. E.A. Stach, T. Freeman, A.M. Minor, D.K. Owen, J. Cumings, M.A. Wall, T. Chraska, R. Hull, J.W. Morris, and A. Zettl, *Microscopy and Microanalysis* **7**, 507 (2001).